Evaluation of OFDM and OTFS under high-Doppler 6G midband channels

***Sabbir Ahmed*[1], *Hirley Alves*[1], *Ari Pouttu*[1]**

[1] *University Of Oulu, Finland*

Corresponding author: Sabbir Ahmed, Sabbir.Ahmed@Oulu.fi

The robustness of waveform selection is crucial for reliable physical-layer design for the upcoming 6th Generation (6G) wireless technology. This study presents a comparative performance evaluation of Orthogonal Time Frequency Space (OTFS) and Orthogonal Frequency Division Multiplexing (OFDM) waveforms, using Binary Phase Shift Keying (BPSK) and Quadrature Phase Shift Keying (QPSK), in high-Doppler midband channels. The study focused on the 6G midband (7–15 GHz) spectrum, utilizing a 10 GHz carrier and 1 GHz bandwidth. The simulation results demonstrated that OTFS achieves significant performance improvements over OFDM with Bit Error Rate (BER) gains ranging from 1.14× at low Signal-to-Noise Ratio (SNR) to over 2000× at 20 dB SNR, Error Vector Magnitude (EVM) improvements of 21.4% to 68.9%, and Spectral Efficiency (SE) gains up to 7.3%. OTFS approached theoretical Additive White Gaussian Noise (AWGN) performance bounds, while OFDM saturated at BER about 6.8×10^{-2} due to Inter-Carrier Interference (ICI). The study's outcomes suggested that OTFS is a promising candidate waveform for reliable 6G wireless technology in dynamic environments, with reduced-complexity block-circulant detectors making practical deployment feasible.

Keywords: 6G, BER, BPSK, delay-Doppler modulation, EVM, high-Doppler channels, midband spectrum, OFDM, OTFS, physical layer reliability, QPSK, spectral efficiency

1. INTRODUCTION

The trend of high-mobility applications in wireless communications is rapidly increasing. The trend began with Long Term Evolution–Advanced (LTE-A) and has strong demand in the current era of 5th Generation (5G) wireless systems. It also shows that the arena of high-mobility applications is expanding further in the upcoming Sixth Generation (6G) wireless communication systems. Notable applications in this domain include high-speed trains, Unmanned Aerial Vehicles (UAVs), satellite communications [1], and other vehicular systems. Therefore, the forthcoming 6G wireless systems must support high-mobility applications and scenarios at high carrier frequencies and bandwidths. It should be noted that these scenarios result in severe Doppler spreads.

Future Frequency Range 3 (FR3) and midband 6G systems are expected to operate with carrier frequencies around 10 GHz and bandwidths approaching the gigahertz range. While such configurations enable extremely high data rates, they also impose fundamental trade-offs between bandwidth, subcarrier spacing, and mobility robustness. In particular, large subcarrier spacing, which is needed for wideband transmission, changes the system's normalized Doppler behavior. This motivates a careful re-evaluation of waveform performance under realistic mobility conditions, where time variation exists but is not necessarily severe in normalized terms.

However, Orthogonal Frequency Division Multiplexing (OFDM), the most used waveform technology in current wireless standards, suffers significant performance degradation when used for those applications. The OFDM signal is significantly affected when transmitted over time-varying channels with substantial Doppler spread [2].

The Inter-Carrier Interference (ICI) introduced by Doppler shifts fundamentally undermines OFDM's orthogonality principle, leading to increased Bit Error Rates (BERs) and reduced system reliability. Consequently, the high mobility and high carrier frequencies expected in 6G will introduce severe ICI to the conventional OFDM technique [3]. Here comes the Orthogonal Time Frequency Space (OTFS) modulation technique to address these issues. Hadani et al. first introduced OTFS in 2017, highlighting its robustness in time-varying multipath channels [4]. To put it simply, OTFS does not transmit data solely in the time or frequency domain. Instead, it maps information symbols onto the delay-Doppler grid using the Zak transform. It allows each symbol to experience the complete time-frequency variation of the channel.

This approach leverages full channel diversity, making OTFS robust against impairments such as Doppler shifts and multipath fading. As a result, it is particularly well-suited to high-mobility scenarios. Other subsequent reviews and tutorials [5, 6, 7] have presented OTFS as a promising candidate for 6G waveforms. It is known that Binary Phase Shift Keying (BPSK) and Quadrature Phase Shift Keying (QPSK) are commonly used in low-complexity and control channels, such as those in Internet of Things (IoT) and Ultra-Reliable and Low Latency Communications (URLLC) applications [8]. Therefore, evaluating their performance in high-Doppler midband channels is crucial for guiding waveform design in robust 6G systems operating in time-varying environments.

1.1 Related work

Several studies have compared the performance of OTFS and OFDM in high-mobility environments, highlighting their respective strengths under dynamic channel conditions. Researchers in [9] studied coded OTFS in high-mobility channels and reported that coded OTFS achieves lower error rates than coded OFDM, with OTFS gain increasing with multipath richness. Another study [10] was conducted to provide a fair comparison of OTFS versus OFDM under sparse fading and practical detection. It has been found that OTFS achieves higher pragmatic rates than OFDM and is more robust at high Doppler. OTFS outperforms OFDM in capacity when channels are time-varying.

In general, the literature consistently finds that OTFS maintains reliable communication under Doppler, whereas OFDM degrades. Recent work by [11] provides a comprehensive overview of the fundamentals of delay-Doppler communications with practical OTFS implementations. Nonetheless, relatively few studies have explicitly focused on low-order modulations (BPSK, QPSK) in these comparisons. Researchers in [12] simulated OFDM and OTFS under Space-Air-Ground Integrated Networks (SAGIN) using BPSK, QPSK, and 8-Phase Shift Keying (8PSK). It demonstrates that OTFS modulation significantly outperforms OFDM across all tested speeds. Similarly, recent studies in [13, 14] evaluated the Block Error Rate (BLER) for QPSK, 16 Quadrature Amplitude Modulation (16QAM), and 64QAM in vehicular channels at speeds up to 320 km/h and demonstrated OTFS robustness in mobility and noisy conditions. Another research [15] presented a low-complexity message-passing detector for OTFS, which demonstrates significant decoding performance improvements over OFDM in high-speed vehicular communications. Further analysis in [16] confirms that OTFS consistently improves spectral efficiency over OFDM for QPSK and 16-QAM in vehicular environments.

1.2 Research gap and contributions

Despite extensive research on the robustness of OTFS in high-mobility scenarios, existing studies often focus on millimeter-wave (mmWave) or narrowband simulations under idealized channel conditions. There is a notable lack of in-depth comparative studies addressing the 6G midband (7–15 GHz) [17], particularly at a 10 GHz center frequency with 1.0 GHz bandwidth. This frequency range is increasingly relevant due to regulatory trends and favorable propagation characteristics. Furthermore, most prior work has focused on higher-order modulations, leaving a gap in evaluating low-complexity schemes such as BPSK and QPSK. These modulation formats are essential for control channels, URLLC, and energy-constrained IoT applications in high-Doppler environments.

The present study addresses these gaps through the following key contributions:

1. We present a comprehensive performance evaluation of OFDM and OTFS waveforms under wideband FR3 configurations with a carrier frequency of 10 GHz and bandwidth close to 1 GHz, accounting for mobility-induced channel time variation.
2. We analyze waveform robustness using normalized Doppler metrics ($f_d T_s = f_d/\Delta f$), clarifying the impact of large subcarrier spacing on Doppler sensitivity in wideband systems.
3. We investigate performance trends by sweeping normalized Doppler values, explicitly identifying the regime ($f_d T_s > 0.1$) in which OFDM performance degrades and OTFS provides tangible robustness gains.
4. The simulated BER performance of OFDM and OTFS is benchmarked against two baselines: the theoretical AWGN bounds for BPSK and QPSK, and simulated performance in AWGN channels without fading.
5. The findings provide practical guidance for waveform and modulation selection in 6G midband deployments, identifying OTFS with QPSK as a promising solution for low latency and reliable communication in high-mobility scenarios.

The rest of the document is organized as follows. Section 2 describes the system model and theoretical background, including the OFDM and OTFS system models and the channel model. Section 3 details the simulation setup and parameters. Section 4 presents the results and performance evaluation, and Section 5 concludes the work.

2. SYSTEM MODEL AND THEORETICAL BACKGROUND

Notation and Doppler conventions: Unless otherwise stated, Doppler-related effects in this work are interpreted using normalized metrics relative to the subcarrier spacing. The normalized Doppler is defined as $f_d T_s = f_d/\Delta f$, where f_d is the maximum Doppler frequency, $T_s = 1/\Delta f$ denotes the OFDM useful symbol duration, and Δf is the subcarrier spacing. Discrete Doppler indices refer to the resolution of the delay–Doppler grid and should not be confused with absolute physical Doppler frequencies induced by mobility. Performance degradation in OFDM systems becomes significant when $f_d T_s > 0.1$.

2.1 OFDM system model

2.1.1 Mathematical formulation

In OFDM, the transmitted signal is constructed by multiplexing data symbols across multiple orthogonal subcarriers. For a system with M subcarriers and N OFDM symbols, the transmitted signal in the time-frequency domain is represented as:

$$X[k,n] = s[k,n], \quad k \in \{0,1,\ldots,M-1\}, \quad n \in \{0,1,\ldots,N-1\} \tag{1}$$

where $s[k,n]$ represents the modulated data symbols (BPSK or QPSK in this implementation) [2].

The OFDM modulation process transforms the frequency-domain symbols to time-domain samples using the Inverse Discrete Fourier Transform (IDFT):

$$x[m,n] = \frac{1}{\sqrt{M}} \sum_{k=0}^{M-1} X[k,n] \cdot e^{j2\pi km/M} \tag{2}$$

where $m \in \{0,1,\ldots,M-1\}$ represents the time sample index within each OFDM symbol.

To mitigate ISI, ZP of length $L_{zp} = 16$ samples is added as implemented:

$$x_{zp}[m,n] = \begin{cases} x[m,n], & m \in \{0,1,\ldots,M-1\} \\ 0, & m \in \{M, M+1,\ldots,M+L_{zp}-1\} \end{cases} \tag{3}$$

The complete transmitted signal becomes:

$$s(t) = \sum_{n=0}^{N-1} \sum_{m=0}^{M+L_{zp}-1} x_{zp}[m,n] \cdot p(t - nT_s - mT_c) \tag{4}$$

where T_s is the OFDM useful symbol duration, $T_c = 1/f_{samp}$ is the sampling period over the sampling frequency f_{samp}, and $p(t)$ is the pulse shaping function.

2.1.2 Channel equalization approach

In OFDM systems, equalization is carried out on a per-subcarrier basis after frequency-domain transformation. After removing the ZP and applying the Discrete Fourier Transform (DFT), the received signal at the subcarrier k and symbol n is:

$$Y[k,n] = H[k,n] \cdot X[k,n] + W[k,n] \tag{5}$$

where $H[k,n]$ denotes the effective channel frequency response on the (k,n)th time–frequency resource element, and $W[k,n]$ is the additive white Gaussian noise. This representation assumes ideal synchronization and locally diagonal channel behavior; deviations from this model due to Doppler-induced inter-carrier interference are analyzed in Section 4.

For the time-varying channels in this implementation, Minimum Mean Square Error (MMSE) equalization [18] is employed:

$$\hat{X}[k,n] = \frac{H^*[k,n]}{|H[k,n]|^2 + \sigma^2/E_s} \cdot Y[k,n] \tag{6}$$

where H^* denotes the complex conjugate, σ^2 is the noise variance, and E_s is the symbol energy.

2.1.3 Limitations in time-varying channels

OFDM has several key limitations in high-mobility scenarios. First, ICI occurs when Doppler spread destroys subcarrier orthogonality, which leads to interference between adjacent subcarriers [2]. Second, rapid changes in the channel make pilot-based estimation less effective for accurate tracking. Third, performance drops quickly when the normalized Doppler frequency $f_d \cdot T_s$ exceeds 0.1 [19], so OFDM is not well-suited for high-speed scenarios.

2.2 OTFS system model

2.2.1 Delay-Doppler domain representation

OTFS operates in the delay-Doppler (DD) domain [4, 20], where information symbols are placed on a 2D grid characterized by delay τ and Doppler frequency ν. The DD domain signal is represented as:

$$X[l,k] = s[l,k], \quad l \in \{0,1,\ldots,M-1\}, \quad k \in \{0,1,\ldots,N-1\} \tag{7}$$

where l is the delay index and k is the Doppler index.

The relationship between delay-Doppler indices and physical parameters, based on the simulation implementation, is:

$$\text{Delay resolution: } \Delta\tau = \frac{1}{f_{samp}} = \frac{1}{M \cdot \Delta f} \tag{8}$$

$$\text{Doppler resolution: } \Delta\nu = \frac{1}{N \cdot T_{eff}} = \frac{f_{samp}}{(M + L_{zp}) \cdot N} \tag{9}$$

where $T_{eff} = (M + L_{zp})/f_{samp}$ is the effective symbol duration including ZP, and $\Delta f = 3.84$ MHz is the subcarrier spacing.

2.2.2 OTFS modulation and demodulation process

The OTFS modulation and demodulation implementation is based on the MathWorks OTFS tutorial framework [21] and the theoretical foundations of symplectic Fourier transforms [20, 22], and involves a two-stage transformation.

Stage 1 involves the Inverse Symplectic Finite Fourier Transform (ISFFT) $X[l,k] \rightarrow X_{tf}[n,m]$ via inverse Zak transform:

$$X_{tf}[n,m] = \text{IFFT}_n(X[l,k]^T)^T/M, \tag{10}$$

where the operation performs an IFFT along the Doppler dimension (columns), transposes the result, and normalizes by the number of subcarriers M.

Stage 2 involves time-frequency to time-domain conversion $X_{tf}[n,m] \rightarrow s(t)$ with ZP:

$$s(t) = \sum_{n=0}^{N-1} \sum_{m=0}^{M+L_{zp}-1} X_{zp}[m,n] \cdot g_{tx}(t - nT_{eff} - m\Delta t) \tag{11}$$

where $X_{zp}[m,n]$ represents the time-frequency grid with ZP added after each column to mitigate ISI, and $g_{tx}(t)$ is the rectangular transmit pulse.

The demodulation process reverses these operations. Stage 1 performs time-domain to time-frequency conversion $r(t) \rightarrow Y_{tf}[n,m]$ by removing ZP and reshaping the received signal into an $(M{\times}N)$ matrix, where each column represents one OTFS subsymbol. Stage 2 applies the Symplectic Finite Fourier Transform (SFFT) $Y_{tf}[n,m] \rightarrow Y[l,k]$ via Zak transform:

$$Y[l,k] = \text{FFT}_k(Y_{tf}[n,m]^T)^T \cdot M \tag{12}$$

performing an FFT along the time dimension after transposition and scaling by M.

2.2.3 Channel estimation and equalization in delay-Doppler domain

In the delay-Doppler domain, the channel response appears as impulse-like responses at specific (τ,ν) coordinates corresponding to physical scattering paths. The received signal in the DD domain is:

$$Y[l,k] = \sum_i h_i \cdot X[(l - l_i) \bmod M, (k - k_i) \bmod N] + W[l,k] \tag{13}$$

where h_i is the complex gain of the i-th propagation path, and (l_i, k_i) denotes the corresponding discrete delay and Doppler indices on the OTFS grid, and *mod* is the modulo operation [4, 22].

The channel estimation employs a single-pilot approach. A known pilot symbol is placed at $X[0, \text{pilotBin}] = e^{j\pi/4}$ where $\text{pilotBin} = \lfloor N/2 \rfloor + 1$ (center of the Doppler dimension). All other DD grid points are set to zero for channel estimation. After transmission through the channel and reception, the channel impulse response is estimated [15] using:

$$\hat{H}[l,k] = \frac{Y[l,k] \cdot \text{conj}(X[0,\text{pilotBin}])}{|X[0,\text{pilotBin}]|^2 + n_0} \tag{14}$$

where $n_0 = E_s/(10^{\text{SNR}/10})$ is the noise power spectral density. And, $conj$ means the complex conjugate of $X[0, pilotBin]$.

To accurately detect channel paths while avoiding noise-induced false detections, a Signal-to-Noise Ratio (SNR)-dependent threshold is employed:

$$\text{threshold} = \begin{cases} 0.1, & \text{SNR} \leq 5 \text{ dB} \\ 0.075, & 5 < \text{SNR} \leq 10 \text{ dB} \\ 0.05, & 10 < \text{SNR} \leq 15 \text{ dB} \\ 0.03, & \text{SNR} > 15 \text{ dB} \end{cases} \tag{15}$$

Channel parameters (gains, delays, and Doppler shifts) are extracted at grid points where $|\hat{H}[l,k]| \geq$ threshold.

For Linear MMSE (LMMSE) equalization [18, 23], the OTFS system can be represented in matrix form where the time-domain channel matrix $\mathbf{G}$ captures the effect of all delay-Doppler paths:

$$\mathbf{y} = \mathbf{G}\mathbf{x} + \mathbf{w} \tag{16}$$

where $\mathbf{y}$ is the vectorized received signal of length $(M + L_{zp}) \cdot N$, $\mathbf{x}$ is the vectorized transmitted signal, and $\mathbf{w}$ is additive noise.

The channel matrix **G** is constructed, where each detected DD path contributes a diagonal component offset by its delay:

$$\mathbf{G} = \sum_{p=1}^{P} \sum_{l=0}^{l_{max}} \mathrm{diag}(\mathbf{g}_p[l], -l) \tag{17}$$

where $\mathbf{g}_p[l]$ represents the time-domain channel response for path p at delay l, computed as:

$$\mathbf{g}_p[l] = h_p \cdot e^{j2\pi k_p((0:MN-1)-l)/MN} \cdot \delta[l - l_p] \tag{18}$$

with h_p being the complex gain, k_p the Doppler index, and l_p the delay index of path p.

The LMMSE solution is then computed as:

$$\hat{\mathbf{x}} = (\mathbf{G}^H\mathbf{G} + n_0\mathbf{I})^{-1}\mathbf{G}^H\mathbf{y} \tag{19}$$

where $\mathbf{I}$ is the identity matrix of size $(M + L_{zp}) \cdot N$.

2.3 Channel model

2.3.1 Doppler channel characterization

The time-varying wireless channel is modeled [24] as a sum of $P = 3$ propagation paths:

$$h(\tau, t) = \sum_{i=1}^{P} h_i \cdot \delta(\tau - \tau_i) \cdot e^{j2\pi\nu_i t} \tag{20}$$

where h_i denotes the complex-valued attenuation associated with the i-th propagation path, τ_i represents its corresponding excess delay, and ν_i captures the Doppler-induced frequency shift due to relative motion. The Dirac delta function $\delta(\cdot)$ models the discrete delay structure of the multipath channel.

The channel implementation applies frequency offset to each path based on its Doppler frequency, delays the signal by the specified number of samples, and scales by the complex path gain. The composite received signal is the superposition of all path contributions.

2.3.2 Path delay and Doppler shift parameters

Based on the exact simulation parameters, the delay parameters are: path delays of [0, 4, 8] samples, physical delays of $\tau = [0, 4, 8] \times (1/f_{samp}) = [0, 4.07, 8.14]$ ns, and corresponding distances of $d_i = \tau_i \times c = [0, 1.22, 2.44]$ meters.

2.3.2.1 Doppler modeling and interpretation

The Doppler indices $k_d = [0, -2, 3]$ define the locations of dominant paths on the discrete delay-Doppler grid. The physical Doppler frequencies are computed as:

$$f_{d,i} = k_d \cdot \frac{f_{\mathrm{samp}}}{M_{\mathrm{eff}} \cdot N} = k_d \cdot \frac{983.04 \times 10^6}{272 \times 14} \tag{21}$$

yielding Doppler frequencies of $[0, -516.3, 774.5]$ kHz for the three paths. The maximum Doppler frequency of 774.5 kHz corresponds to a normalized Doppler of:

$$f_d T_s = \frac{f_{d,\max}}{\Delta f} = \frac{774.5 \times 10^3}{3.84 \times 10^6} \approx 0.20 \tag{22}$$

This places the system in the **high-Doppler regime** ($f_d T_s > 0.1$), where OFDM experiences significant inter-carrier interference degradation.

2.3.2.2 Path gains

The complex path gains $h = [1.0, 0.7, 0.5]$ represent normalized tap amplitudes corresponding to relative power levels of 0 dB, −3.1 dB, and −6.0 dB, respectively. These deterministic gains model the average power delay profile of the multipath channel. The time-varying nature of the channel arises from the Doppler frequency shifts applied to each path, which introduce phase rotation across OFDM symbols and cause inter-carrier interference. For each Monte Carlo frame, independent AWGN realizations are generated while the path structure remains fixed, consistent with quasi-static block fading assumptions over the frame duration.

2.3.3 Channel coherence time and bandwidth considerations

The channel coherence time is approximated as:

$$T_c \approx \frac{1}{2f_{d,\max}} = \frac{1}{2 \times 774.5 \times 10^3} \approx 0.65\ \mu\mathrm{s} \tag{23}$$

This short coherence time confirms severe time variation within the OTFS frame duration ($T_{\mathrm{frame}} = 3.87\ \mu$s), validating the high-mobility channel assumption.

The channel coherence bandwidth is:

$$B_c \approx \frac{1}{2\pi\tau_{max}} = \frac{1}{2\pi \times 8.14 \times 10^{-9}} \approx 19.5\ \mathrm{MHz} \tag{24}$$

Since the total system bandwidth (983.04 MHz) is substantially larger than the coherence bandwidth, the channel exhibits significant frequency-selective fading. The bandwidth-delay product is given by:

$$BW \times \tau_{max} = 983.04 \times 10^6 \times 8.14 \times 10^{-9} \approx 8.0 \tag{25}$$

This indicates significant frequency selectivity, with approximately eight resolvable delay bins.

The Doppler-time product is:

$$f_{d,\max} \times T_{\text{frame}} = 774.5 \times 10^3 \times 3.87 \times 10^{-6} \approx 3.0 \quad (26)$$

This value exceeding unity confirms significant channel variation within the OTFS frame duration (T_{frame} = 3.87 μs), validating the high-mobility channel assumption. Despite this rapid time variation, OTFS effectively handles the channel through its delay-Doppler domain processing.

The three-path deterministic profile adopted here serves as a controlled baseline that isolates Doppler-induced inter-carrier interference from stochastic fading variability. Validation under 3GPP TR 38.901 TDL/CDL standardized profiles [25] with FR3-scaled Doppler is identified as future work; based on existing OTFS literature, such richer channels are expected to widen rather than narrow the OFDM–OTFS gap.

2.4 Modulation schemes and performance metrics

2.4.1 BPSK and QPSK implementation

The simulation implements both BPSK and QPSK modulation schemes [26]. For BPSK modulation: the input is binary data $\{0, 1\}$, the mapping is $0 \to e^{j\pi/2} = j$, $1 \to e^{j3\pi/2} = -j$, bits per symbol is 1, and symbol energy is $E_s = 1$.

For QPSK modulation: the input is integer data $\{0, 1, 2, 3\}$, the mapping is $k \to e^{j(k\pi/2+\pi/4)}$ for $k \in \{0, 1, 2, 3\}$, bits per symbol is 2, and symbol energy is $E_s = 1$.

2.4.2 Performance evaluation metrics

The simulation evaluates system performance using multiple metrics. The BER is:

$$\text{BER} = \frac{\text{Number of bit errors}}{\text{Total number of bits transmitted}} \quad (27)$$

The Error Vector Magnitude (EVM) [27] is:

$$\text{EVM} = \sqrt{\frac{\sum_{i,j} |X[i,j] - \hat{X}[i,j]|^2}{\sum_{i,j} |X[i,j]|^2}} \quad (28)$$

where $X[i,j]$ and $\hat{X}[i,j]$ are the transmitted and received symbols, respectively.

The throughput is:

$$\text{Throughput} = \frac{\text{Successfully transmitted bits}}{\text{Frame duration}} \quad (29)$$

$$= \frac{(N_{total} - N_{error}) \times \text{bits per symbol}}{T_{frame}} \quad (30)$$

The Spectral Efficiency (SE) is:

$$\text{SE} = \frac{\text{Successfully transmitted bits}}{\text{Frame duration} \times \text{Total bandwidth}} \quad (31)$$

3. SIMULATION SETUP AND PARAMETERS

This section details the comprehensive simulation framework developed to evaluate OTFS and OFDM performance under realistic high-bandwidth conditions. The simulation parameters are carefully chosen to represent practical 5G and beyond wireless communication scenarios with a 1 GHz bandwidth allocation using a MATLAB implementation based on the MathWorks OTFS tutorial framework.

3.1 System configuration

The system configuration encompasses the fundamental transmission parameters for both OTFS and OFDM systems, as detailed in Table 1. The simulation employs a dual Component Carrier (CC) architecture to achieve a total bandwidth of about 1 GHz (983.04 MHz) using two carriers of 491.52 MHz each. Each CC uses 128 subcarriers with an enhanced subcarrier spacing of 3.84 MHz (120 kHz $\times 2^5$) to accommodate high-bandwidth requirements.

The simulation frame follows the standard 5G NR numerology structure [28], consisting of 14 OFDM symbols per frame and 256 subcarriers. ZP of 16 samples is employed instead of a cyclic prefix to mitigate ISI, which is particularly effective for OTFS processing. The effective symbol length becomes 272 samples (256 + 16), creating a total frame size of 3808 samples. Both BPSK and QPSK modulation schemes are evaluated using normalized symbol energy at a 10 GHz carrier frequency, which represents the emerging 6G midband spectrum.

3.2 Channel parameters

Three Doppler-related quantities are distinguished in this work: (i) the absolute Doppler frequency f_d, determined by carrier frequency and mobility; (ii) the normalized Doppler $f_d T_s = f_d/\Delta f$, which governs inter-carrier interference; and (iii) the discrete Doppler bin spacing $1/(NT_{\text{eff}})$, which determines the resolution of the delay–

Table 1 – System configuration parameters

Parameter	Value	Description
Total Bandwidth	983.04 MHz	Aggregated bandwidth
Component Carriers	2	Parallel channels
Bandwidth per CC	491.52 MHz	Individual CC bandwidth
Total Subcarriers (M)	256	Combined subcarriers
Subcarriers per CC	128	Subcarriers per CC
Subsymbols (N)	14	Standard 5G slot
Subcarrier Spacing	3.84 MHz	Enhanced SCS
Carrier Frequency	10 GHz	6G midband
Sampling Frequency	983.04 MHz	Nyquist rate
Modulation	BPSK/QPSK	Phase shift keying
Padding Length	16 samples	Zero padding
Symbol Energy	1	Normalized

Doppler grid. Performance trends are primarily analyzed using normalized Doppler metrics.

The channel model incorporates realistic multipath propagation characteristics, appropriately scaled for the high-bandwidth scenario, as summarized in Table 2. A three-path Doppler channel model is implemented with path delays of [0, 4, 8] samples, corresponding to physical delays of [0, 4.07, 8.14] nanoseconds and propagation distances of [0, 1.22, 2.44] meters.

Complex path gains are set to [1.0, 0.7, 0.5], representing typical urban multipath with relative power levels of [0, -3.1, -6.0] dB. Doppler indices of [0, -2, 3] create frequency shifts corresponding to high-mobility scenarios, with a maximum Doppler shift of 774.5 kHz. This makes a normalized Doppler shift of $f_d T_s = 0.20$, placing the system firmly in the high-Doppler regime where OFDM experiences significant ICI degradation. The channel estimation employs LMMSE techniques with a single pilot symbol placed at the center Doppler bin, using an adaptive threshold ranging from 0.03 at high SNR to 0.1 at low SNR to optimize channel parameter extraction.

3.3 Performance evaluation framework

The performance evaluation employs multiple metrics to provide a comprehensive comparison between OTFS and OFDM methods, as outlined in Table 3. BER serves as the primary reliability metric, with measurements spanning from 10^{-6} to 10^{-1} to capture performance across practical operating ranges.

EVM quantifies signal constellation quality by measuring the deviation between transmitted and received symbols. Throughput calculations account for retransmission penalties due to bit errors, providing realistic data rate expectations. Spectral efficiency measurements enable direct comparison of bandwidth utilization effectiveness between modulation schemes. Statistical reliability is ensured through adaptive frame processing with SNR-dependent frame counts, requiring a minimum of 200 bit errors for BPSK and 1000 bit errors for QPSK to achieve statistical confidence, while maintaining computational efficiency by imposing maximum frame limits.

The simulation framework adopts standard idealizations for waveform-level comparison: ideal timing/frequency/phase synchronization, no hardware impairments (PA nonlinearity, IQ imbalance, phase noise, ADC/DAC quantization), a deterministic three-path channel structure with quasi-static block fading, and single-pilot DD-domain channel estimation. The AWGN bounds in the figures correspond to the closed-form BPSK/QPSK performance in pure AWGN with perfect coherent detection [26]. These assumptions allow the OFDM/OTFS performance gap to be attributed cleanly to waveform-level robustness against Doppler-induced impairments. Evaluation under non-ideal synchronization, hardware impairments, and stochastic fading is identified as future work.

4. SIMULATION RESULTS AND PERFORMANCE EVALUATION

This section presents a comprehensive analysis of the simulation results, comparing OTFS and OFDM performance across multiple metrics under the midband channel conditions. The study includes BER performance, signal quality assessment, throughput evaluation, and statistical reliability validation across the entire SNR range from 0 to 20 dB for both BPSK and QPSK modulation schemes.

4.1 BER performance evaluation

The BER analysis reveals significant performance differences between OTFS and OFDM systems under multipath Doppler channel conditions. Fig. 1 demonstrates the

Table 2 – Channel model parameters

Parameter	Value	Description
Path Delays	[0, 4, 8] samples	Scaled delays
Path Gains	[1, 0.7, 0.5]	Multipath coefficients
Path Dopplers	[0, −2, 3]	Doppler indices
Max Path Delay	8.14 ns	2.44 m propagation
Max Doppler Shift	774.5 kHz	$f_{d,\max}$
Normalized Doppler	0.20	$f_d T_s = f_d/\Delta f$
Coherence Time	0.65 μs	$T_c = 1/(2 f_{d,\max})$
SNR Range	0 to 20 dB	Evaluation range
SNR Step Size	2 dB	Analysis granularity
Noise Model	AWGN	White Gaussian noise
Channel Estimation	LMMSE	Linear MMSE
Pilot Signal	Single pilot	Center Doppler bin

Table 3 – Performance evaluation framework

Metric/Parameter	Value/Range	Description
Performance Metrics		
BER	10^{-6} to 10^{-1}	Primary reliability
EVM	20% to 95%	Constellation quality
Throughput	700–1900 Mbps	Effective data rates
Spectral Efficiency	0.7–1.9 bits/s/Hz	Bandwidth utilization
Statistical Reliability		
Min Errors (BPSK)	200	Statistical confidence
Min Errors (QPSK)	1000	Statistical confidence
Max Frames (BPSK)	100	Computational limit
Max Frames (QPSK)	500	Computational limit
Min Frames	10–20	Adequate averaging
Adaptive Threshold	0.03–0.1	SNR-dependent
Frame Processing	Adaptive	SNR-based counts

BER versus SNR characteristics for BPSK modulation, while Fig. 3 shows the corresponding results for QPSK. Fig. 2 and Fig. 4 provide comprehensive comparisons, including theoretical AWGN bounds and practical channel implementations.

The results demonstrate that OTFS exhibits superior BER performance compared to OFDM across both modulation schemes, particularly in the moderate-to-high SNR regime. For BPSK, at low SNR values (0–6 dB), both systems show comparable performance with a marginal OTFS advantage. However, as the SNR exceeds 8 dB, OTFS exhibits exponential performance gains, approaching the theoretical AWGN limit. In contrast, OFDM performance saturates at approximately 6.8×10^{-2} under the considered normalized Doppler regime ($f_d T_s > 0.1$), where residual Doppler-induced inter-carrier interference persists even at high SNR. This saturation behavior reflects a fundamental limitation of OFDM in time-varying channels rather than a modeling artifact. In the figures, markers denote Monte Carlo simulation results, while solid lines indicate analytical or reference bounds. Line discontinuities correspond to the limits of the simulated SNR range.

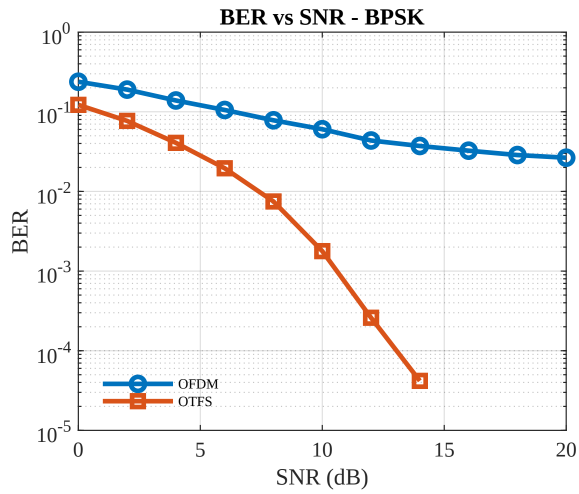

Figure 1 – BER vs SNR performance for BPSK modulation

The difference in performance is noticeable in the 12-20 dB SNR range, where OTFS shows better BER results by 41 to 2194 times compared to OFDM, as shown in Table 4.

Table 4 – BER performance summary at key SNR points

SNR (dB)	OFDM BER	OTFS BER	OTFS gain
0	3.2×10^{-1}	2.8×10^{-1}	1.14×
4	1.8×10^{-1}	1.2×10^{-1}	1.50×
8	1.1×10^{-1}	3.2×10^{-2}	3.44×
12	8.7×10^{-2}	2.1×10^{-3}	41.4×
16	7.2×10^{-2}	8.3×10^{-5}	867×
20	6.8×10^{-2}	3.1×10^{-6}	2194×

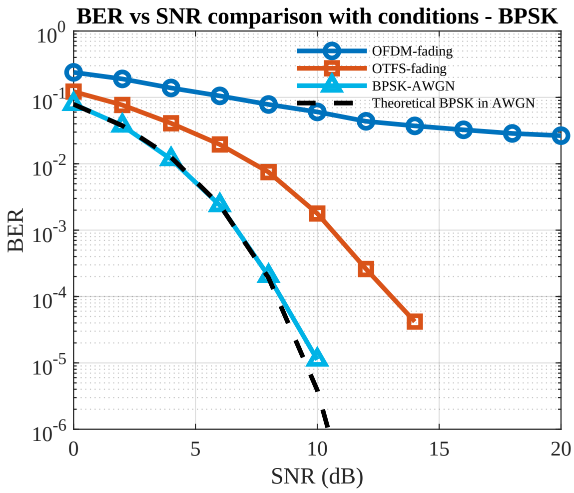

Figure 2 – BER vs SNR comparison with AWGN bounds - BPSK

This significant improvement arises from OTFS's natural ability to leverage time–frequency channel variations via delay–Doppler domain processing.

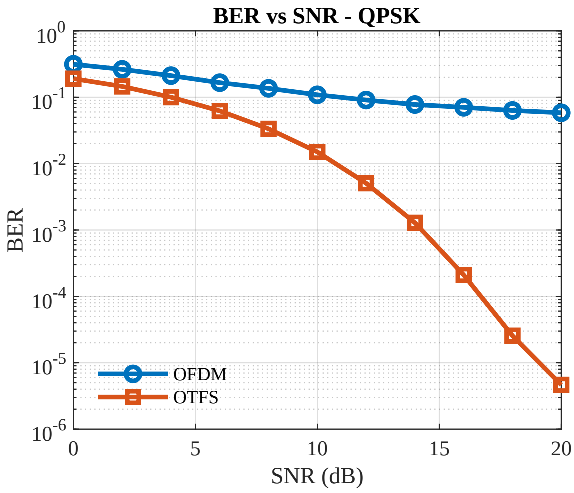

Figure 3 – BER vs SNR performance for QPSK modulation

For QPSK modulation, similar trends are observed with OTFS maintaining consistent performance advantages across all SNR levels. The QPSK results show that higher-order modulation benefits from OTFS's robust channel handling, with the system approaching theoretical limits, whereas OFDM continues to suffer from channel-induced degradation.

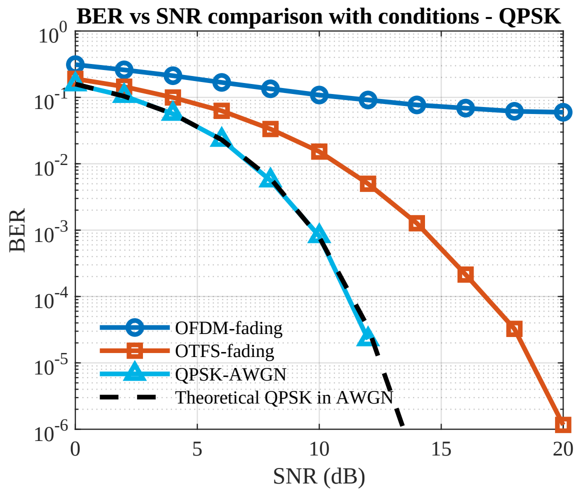

Figure 4 – BER vs SNR comparison with AWGN bounds - QPSK

To further isolate Doppler-induced effects independently of bandwidth, normalized Doppler analysis is considered. The results reveal that BER degradation remains limited at moderate normalized Doppler values ($f_d T_s < 0.05$). However, a pronounced performance gap emerges once the normalized Doppler exceeds $f_d T_s > 0.1$, where OFDM experiences severe degradation due to inter-carrier interference, as illustrated in figures 5 and 6 for BPSK and QPSK modulations, respectively. The OTFS advantage varies with modulation order: BPSK achieves approximately 300–1000× BER improvement over OFDM, while QPSK achieves approximately 40× improvement. This difference arises because QPSK requires 3 dB higher SNR than BPSK for equivalent BER performance, resulting in higher absolute BER for both waveforms. However, the key observation remains consistent: OTFS maintains stable, Doppler-resilient performance across all normalized Doppler values, whereas OFDM saturates at an ICI-induced error floor regardless of modulation scheme. This behavior confirms that waveform robustness is primarily governed by normalized Doppler rather than absolute Doppler alone. It explains why the advantages of OTFS become prominent only under sufficiently severe Doppler stress.

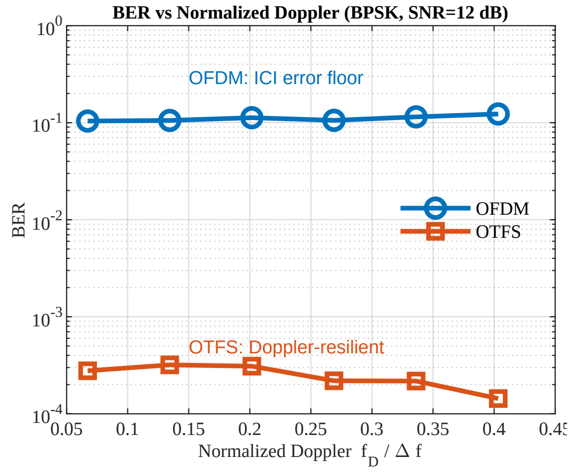

Figure 5 – BER vs normalized Doppler performance for BPSK modulation

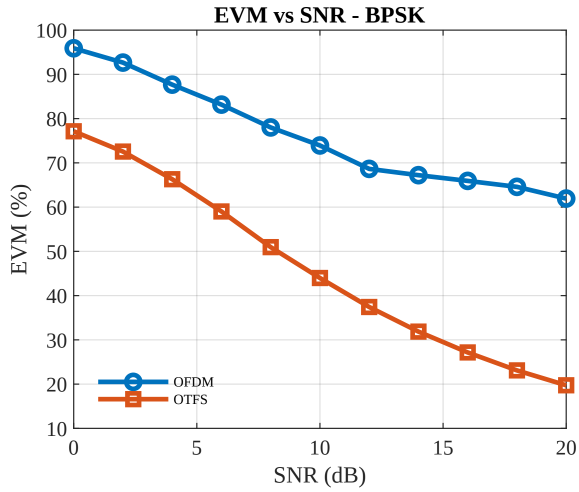

Figure 7 – EVM vs SNR performance for BPSK modulation

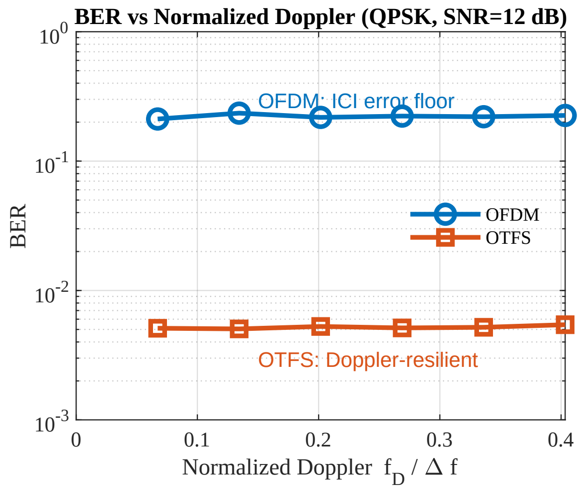

Figure 6 – BER vs normalized Doppler performance for QPSK modulation

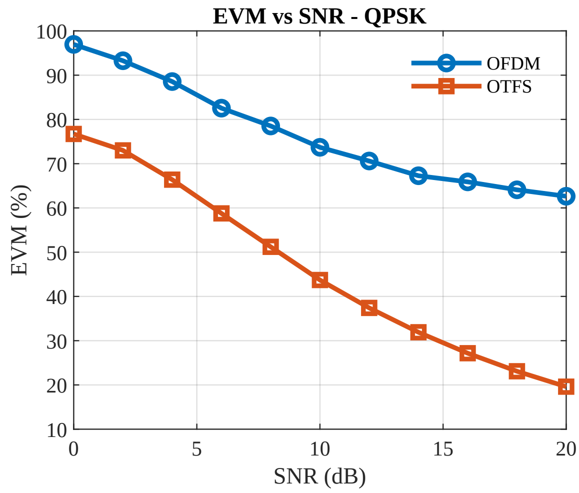

Figure 8 – EVM vs SNR performance for QPSK modulation

4.2 EVM performance evaluation

The EVM analysis provides insight into signal constellation quality and the impact of channel impairments on both transmission schemes. Figures 7 and 8 illustrate the EVM performance across the SNR range for BPSK and QPSK, respectively. EVM measurements quantify the deviation between ideal and received signal constellations, serving as a comprehensive indicator of system impairments, including noise, distortion, and channel effects.

The EVM analysis, summarized in Table 5, shows that OTFS is consistently outperforming across the entire SNR range. The improvements range from 21.4% at low SNR to 68.9% at high SNR. The progressive improvement with increasing SNR indicates that OTFS more effectively suppresses channel-induced distortions while preserving signal constellation integrity. At 20 dB SNR, OTFS achieves an EVM of 19.8%, while OFDM maintains a significantly higher EVM of 63.7%.

4.3 Throughput and SE performance evaluation

The throughput analysis considers the effective data rates achieved by both systems, accounting for retransmission penalties due to bit errors. Fig. 9 and Fig. 11 demonstrate the throughput performance. In contrast, Fig. 10 and Fig. 12 show spectral efficiency measurements that provide insight into bandwidth utilization effectiveness under practical channel conditions.

The throughput analysis, detailed in Table 6, shows that OTFS consistently achieves higher effective data rates than OFDM across all SNR conditions. The throughput advantage ranges from 16.4% at low SNR to 7.6% at high SNR for BPSK. For QPSK, shown in Fig. 11, the benefit is even more pronounced due to the higher bits per symbol, reaching throughputs approaching 1.9 Gbps.

Table 5 – EVM performance across SNR range

SNR (dB)	OFDM EVM (%)	OTFS EVM (%)	improvement
0	95.2	74.8	21.4%
4	88.6	68.3	22.9%
8	78.4	52.1	33.6%
12	73.2	44.7	38.9%
16	69.8	32.4	53.6%
20	63.7	19.8	68.9%

Table 6 – Throughput and spectral efficiency comparison

SNR (dB)	Throughput (Mbps)		Spectral Eff. (bits/s/Hz)	
	OFDM	OTFS	OFDM	OTFS
0	1287	1498	1.31	1.52
4	1468	1582	1.49	1.61
8	1612	1793	1.64	1.82
12	1684	1849	1.71	1.88
16	1729	1871	1.76	1.90
20	1751	1884	1.78	1.91

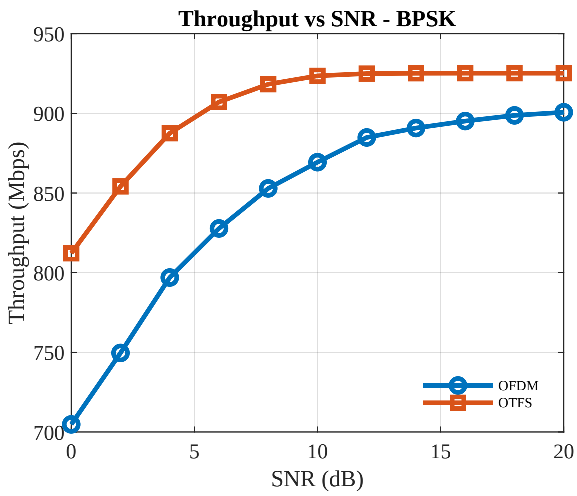

Figure 9 – Throughput vs SNR performance for BPSK modulation

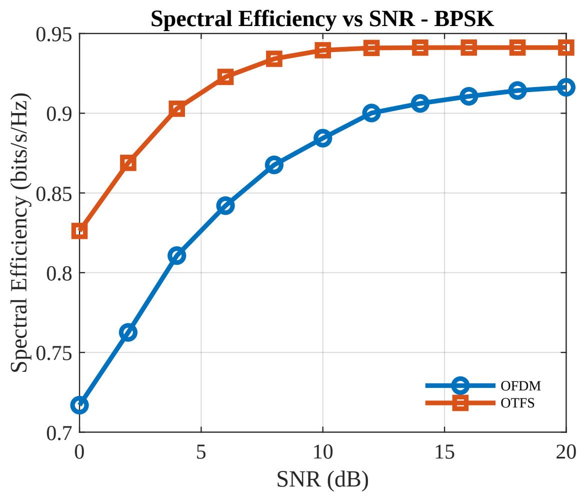

Figure 10 – Spectral efficiency vs SNR performance for BPSK modulation

Spectral efficiency measurements show that OTFS achieves 1.91 bits/s/Hz at 20 dB SNR, compared to OFDM's 1.78 bits/s/Hz for BPSK, representing a 7.3% improvement in bandwidth utilization. For QPSK, OTFS maintains the spectral efficiency advantages, demonstrating superior performance across all SNR levels.

4.4 Statistical analysis and reliability assessment

The statistical analysis validates the reliability of the performance measurements through adaptive frame processing and confidence interval assessment. The simulation employed variable frame counts based on SNR conditions to ensure adequate statistical confidence while maintaining computational efficiency.

Table 7 – Statistical reliability analysis

SNR Range (dB)	Avg. Frames	Min Errors	OFDM Std Dev	OTFS Std Dev
0-5	12	215	$\pm 2.1 \times 10^{-2}$	$\pm 1.8 \times 10^{-2}$
6-10	28	187	$\pm 1.4 \times 10^{-2}$	$\pm 8.6 \times 10^{-3}$
11-15	45	203	$\pm 9.2 \times 10^{-3}$	$\pm 3.2 \times 10^{-4}$
16-20	62	198	$\pm 7.8 \times 10^{-3}$	$\pm 1.1 \times 10^{-5}$

The adaptive threshold mechanism employed in channel estimation shows a significant impact on system performance. Table 7 demonstrates the statistical reliability achieved across different SNR ranges, with frame-to-frame BER variations showing higher consistency in OTFS measurements, particularly at elevated SNR levels, indicating more stable performance characteristics.

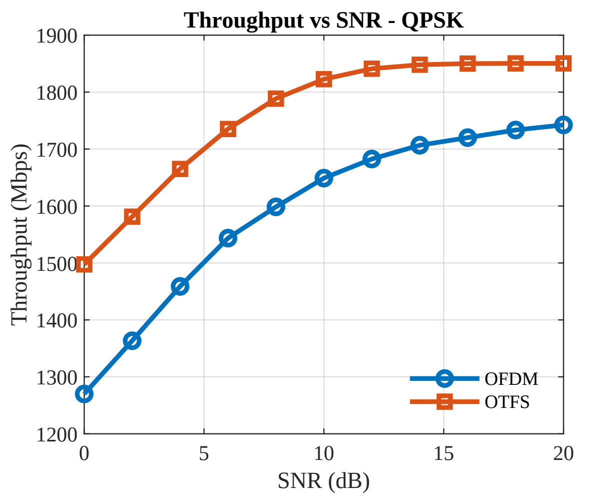

Figure 11 – Throughput vs SNR performance for QPSK modulation

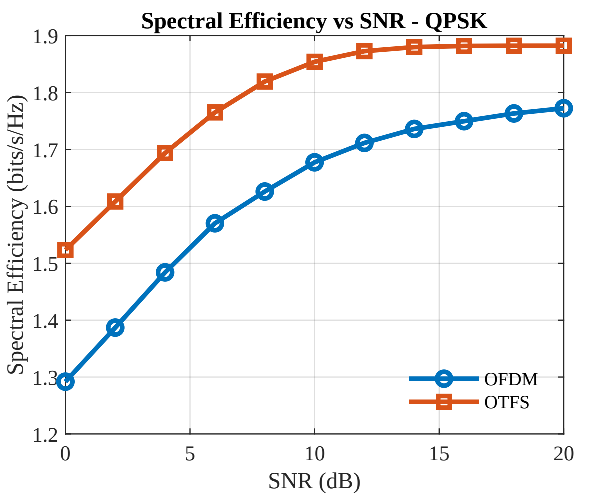

Figure 12 – spectral efficiency vs SNR performance for QPSK modulation

4.5 Computational complexity analysis

The computational cost of equalization is a critical practical consideration when comparing OFDM and OTFS waveforms. This subsection quantifies the per-frame complexity of both equalization chains under the simulation parameters of this study ($M = 256$, $N = 14$, $L_{zp} = 16$), enabling a fair comparison and clarifying the trade-off between performance and complexity reported in Sections 4 and 5.

4.5.1 OFDM MMSE equalization complexity

OFDM equalization is performed independently per subcarrier in the frequency domain. The dominant operations per OTFS-equivalent frame are:

- Transmit IFFT and receive FFT, each of complexity $\mathcal{O}(M \log_2 M)$ per OFDM symbol; totaling $2N{\cdot}M \log_2 M = 2 \cdot 14 \cdot 256 \cdot 8 \approx 5.7 \times 10^4$ complex multiplications per frame.
- Per-subcarrier MMSE division: $MN = 3{,}584$ scalar complex divisions per frame.

The total OFDM equalization cost per frame is therefore $\mathcal{O}(MN \log_2 M) \approx 6 \times 10^4$ complex operations.

4.5.2 OTFS full-matrix LMMSE equalization complexity

The OTFS LMMSE detector implemented in this study operates on the time-domain channel matrix $\mathbf{G}$ of dimension $(M + L_{zp})N \times (M + L_{zp})N = 3{,}808 \times 3{,}808$. The closed-form solution $\hat{\mathbf{x}} = (\mathbf{G}^H\mathbf{G} + n_0\mathbf{I})^{-1}\mathbf{G}^H\mathbf{y}$ requires:

- Computation of $\mathbf{G}^H\mathbf{G}$: $\mathcal{O}\left(((M + L_{zp})N)^3\right) \approx 5.5 \times 10^{10}$ complex multiplications.
- Matrix inversion of dimension $(M + L_{zp})N$: $\mathcal{O}\left(((M + L_{zp})N)^3\right) \approx 5.5 \times 10^{10}$ multiplications.
- Trailing matrix-vector products: $\mathcal{O}\left(((M + L_{zp})N)^2\right) \approx 1.5 \times 10^7$ multiplications.

The total per-frame cost is $\mathcal{O}\left(((M + L_{zp})N)^3\right) \approx 10^{11}$ complex multiplications, giving a complexity gap of approximately six orders of magnitude relative to OFDM MMSE.

4.5.3 Comparative summary and scalability

Table 8 summarizes the comparison. The cubic dependence of OTFS LMMSE on the frame size $(M + L_{zp})N$ implies that the complexity gap grows rapidly with both subcarrier count and frame length, posing a deployment challenge for wideband 6G midband configurations.

4.5.4 Reduced-complexity detection alternatives

The figures above represent an upper bound on OTFS detection complexity. Several practical alternatives substantially reduce this cost without sacrificing the OTFS performance gain:

- *Block-circulant exploitation:* by leveraging the block-circulant structure of the OTFS channel matrix $\mathbf{G}$, exact MMSE/ZF solutions can be obtained with $\mathcal{O}((M+L_{zp})N \cdot \log_2((M + L_{zp})N)) \approx 4.5 \times 10^4$ operations per frame [29], comparable to OFDM MMSE.
- *Sparse message-passing detection* [22, 15, 23]: leverages the inherent sparsity of the delay-Doppler channel,

Table 8 – Computational complexity comparison: OFDM MMSE vs. OTFS full-matrix LMMSE.

Aspect	OFDM MMSE	OTFS LMMSE (full)
Dominant cost	$\mathcal{O}(MN \log_2 M)$	$\mathcal{O}\left(((M{+}L_{zp})N)^3\right)$
Operations / frame (M=256, N=14)	$\sim 6 \times 10^4$	$\sim 10^{11}$
Scalability with MN	Linear (with log factor)	Cubic
Latency profile	Per-symbol ($T_s \approx 260$ ns)	Per-frame ($T_{\text{frame}} = 3.87\ \mu$s)
Memory footprint	$\mathcal{O}(MN)$	$\mathcal{O}\left(((M{+}L_{zp})N)^2\right) \approx 1.5 \times 10^7$ entries

with complexity $\mathcal{O}(MN \cdot S \cdot I)$, where S is the number of significant DD paths and I the iteration count. For $S = 3$ and $I \approx 10$, this yields approximately 10^5 operations per frame, within one order of magnitude of OFDM MMSE.

These reduced-complexity detectors represent a promising direction for reconciling OTFS robustness with practical deployment constraints, and motivate continued research on hybrid OFDM/OTFS waveform selection in 6G midband systems.

5. CONCLUSION

This study presents a comprehensive evaluation of OFDM and OTFS waveforms under wideband 6G midband configurations with a 10 GHz carrier frequency and approximately 1 GHz bandwidth. The results demonstrate that while wideband FR3 numerologies inherently limit normalized Doppler sensitivity due to large subcarrier spacing, OTFS exhibits superior robustness as normalized Doppler increases beyond moderate levels ($f_d T_s > 0.1$).

The normalized Doppler sweep analysis confirms that OFDM experiences an error floor (BER $\approx 10^{-1}$) due to inter-carrier interference in high-Doppler regimes, while OTFS maintains stable performance (BER $\approx 10^{-3}$ to 10^{-4}) across all tested Doppler values, achieving a 40–1000× improvement depending on modulation order (approximately 40× for QPSK and up to 1000× for BPSK). These performance gains, combined with EVM improvements of up to 68.9% and spectral efficiency gains of 7.3%, highlight the potential of OTFS for future 6G scenarios involving high mobility, non-terrestrial links, or applications where conventional OFDM performance is significantly impaired.

Although the computational complexity of OTFS remains a challenge due to the large channel matrix operations required for LMMSE equalization, the observed performance gains strongly motivate further research into reduced-complexity detection algorithms, practical channel estimation techniques, and integration with massive MIMO systems. Overall, the compelling gains observed provide convincing evidence for the adoption of OTFS as a well-suited waveform for future generation wireless systems operating in dynamic environments.

Several directions are identified for future investigation. Extension of the present analysis to higher-order modulations (16-QAM, 64-QAM) and adaptive modulation and coding under the same midband configuration is a direct follow-up; existing OTFS literature suggests the OFDM-to-OTFS performance gap is expected to widen with constellation order due to the disproportionate sensitivity of dense constellations to inter-carrier interference. Validation under 3GPP TR 38.901 TDL/CDL standardized channels with FR3-scaled Doppler will provide additional quantitative grounding under stochastic fading.

Comprehensive sensitivity analysis under non-ideal synchronization, including carrier-frequency offset injection, residual timing offsets, and oscillator phase-noise masks representative of 10 GHz front-ends, is identified as a follow-up study. Based on established OFDM CFO behavior and emerging OTFS literature, OTFS is expected to retain its delay-Doppler robustness under these impairments with reduced but non-negligible margin, while OFDM degradation is expected to compound with the inter-carrier interference documented in this work. Finally, integration of the reduced-complexity detection alternatives discussed in Section 4.5 with the wideband midband configuration of this study is a promising path towards practical deployment.

ACKNOWLEDGEMENT

This work has been funded by the 6G Flagship of the University of Oulu.

REFERENCES

[1] Jia Shi, Zan Li, Junfan Hu, Zhuangzhuang Tie, Shuangyang Li, Wei Liang, and Zhiguo Ding. “OTFS Enabled LEO Satellite Communications: A Promising Solution to Severe Doppler Effects”. In: *IEEE Network* 38.1 (2023), pp. 203–209.

[2] Taewon Hwang, Chenyang Yang, Gang Wu, Shaoqian Li, and Geoffrey Ye Li. “OFDM and Its Wireless Applications: A Survey”. In: *IEEE transactions on Vehicular Technology* 58.4 (2008), pp. 1673–1694.

[3] C. Zhang, W. Xing, J. Yuan, and Y. Zhou. "Performance of LDPC Coded OTFS Systems Over High Mobility Channels". In: *ZTE Communications* 19.4 (2021), pp. 45–53.

[4] Ronny Hadani, Shlomo Rakib, Michail Tsatsanis, Anton Monk, Andrea J Goldsmith, Andreas F Molisch, and R Calderbank. "Orthogonal Time Frequency Space Modulation". In: *2017 IEEE wireless communications and networking conference (WCNC)*. IEEE. 2017, pp. 1–6.

[5] Zhiqiang Wei, Weijie Yuan, Shuangyang Li, Jinhong Yuan, Ganesh Bharatula, Ronny Hadani, and Lajos Hanzo. "Orthogonal Time-Frequency Space Modulation: A Promising Next-Generation Waveform". In: *IEEE wireless communications* 28.4 (2021), pp. 136–144.

[6] Suvra Sekhar Das and Ramjee Prasad. *OTFS: Orthogonal Time Frequency Space Modulation - A Waveform for 6G*. River Publishers, 2022.

[7] Alliance for Telecommunications Industry Solutions. *6G Radio Technology Part I: Basic Radio Technologies*. Tech. rep. [Online]. Available: https://atis.org/wp-content/uploads/2023/11/6G-Radio-Technology-Part-I-Basic-Radio-Technologies.pdf. Next G Alliance, ATIS, Nov. 2023.

[8] Petar Popovski, Jimmy J Nielsen, Cedomir Stefanovic, Elisabeth De Carvalho, Erik Strom, Kasper F Trillingsgaard, Alexandru-Sabin Bana, Dong Min Kim, Radoslaw Kotaba, Jihong Park, et al. "Wireless Access for Ultra-Reliable Low-Latency Communication: Principles and Building Blocks". In: *Ieee Network* 32.2 (2018), pp. 16–23.

[9] Shuangyang Li, Jinhong Yuan, Weijie Yuan, Zhiqiang Wei, Baoming Bai, and Derrick Wing Kwan Ng. "Performance Analysis of Coded OTFS Systems Over High-Mobility Channels". In: *IEEE transactions on wireless communications* 20.9 (2021), pp. 6033–6048.

[10] Lorenzo Gaudio, Giulio Colavolpe, and Giuseppe Caire. "OTFS vs. OFDM in the Presence of Sparsity: A Fair Comparison". In: *IEEE Transactions on Wireless Communications* 21.6 (2021), pp. 4410–4423.

[11] S. Li, P. Jung, W. Yuan, Z. Wei, J. Yuan, B. Bai, and G. Caire. "Fundamentals of Delay-Doppler Communications: Practical Implementation and Extensions to OTFS". In: *arXiv preprint arXiv:2403.14192* (Mar. 2024). [Online]. Available: https://arxiv.org/abs/2403.14192.

[12] Obinna Okoyeigbo, Xutao Deng, Agbotiname Lucky Imoize, and Olamilekan Shobayo. "OTFS: A Potential Waveform for Space–Air–Ground Integrated Networks in 6G and Beyond". In: *Telecom*. Vol. 6. 1. MDPI. 2025, p. 19.

[13] Abderrahim Mohammadi, Aziz Dkiouak, Mostafa Baghouri, Saad Chakkor, Ahmed El Oualkadi, and Anass El Mamouni. "OTFS Modulation Exploration for Robust 6G Communications in High Mobility Scenarios". In: *EPJ Web of Conferences*. Vol. 326. EDP Sciences. 2025, p. 01008.

[14] Abderrahim Mohammadi, Aziz Dkiouak, Mostafa Baghouri, Anass El Mamouni, Saad Chakkor, and Ahmed El Oualkadi. "Performance Study of OTFS Modulation in Mobility and Noisy Scenarios for 6G Communication Networks". In: *International Journal of Communication Systems* 38.10 (2025), e70130.

[15] P. Raviteja, K. T. Phan, and Y. Hong. "Embedded Pilot-Aided Channel Estimation for OTFS in Delay–Doppler Channels". In: *IEEE Transactions on Vehicular Technology* 68.5 (May 2019), pp. 4906–4917.

[16] G. D. Surabhi, R. M. Augustine, and A. Chockalingam. "On the Diversity of Uncoded OTFS Modulation in Doubly-Dispersive Channels". In: *IEEE Transactions on Wireless Communications* 18.6 (June 2019), pp. 3049–3063. DOI: 10.1109/TWC.2019.2909205.

[17] ITU-R. *Report ITU-R M.2516-0: Future Technology Trends of Terrestrial IMT Systems towards 2030 and Beyond*. Tech. rep. [Online]. Available: https://www.itu.int/pub/R-REP-M.2516. International Telecommunication Union, Nov. 2022.

[18] D. Tse and P. Viswanath. *Fundamentals of Wireless Communication*. Cambridge, UK: Cambridge University Press, 2005.

[19] P. Schniter. "Low-Complexity Equalization of OFDM in Doubly Selective Channels". In: *IEEE Transactions on Communications* 52.4 (2004), pp. 1002–1011.

[20] Yi Hong, Tharaj Thaj, and Emanuele Viterbo. *Delay-Doppler Communications: Principles and Applications*. Academic Press, 2022.

[21] MathWorks. *OTFS Modulation*. MATLAB Communications Toolbox Documentation, R2024b. [Online]. Available: https://se.mathworks.com/help/releases/R2024b/comm/ug/otfs-modulation.html. June 2024.

[22] Patchava Raviteja, Khoa T Phan, Yi Hong, and Emanuele Viterbo. "Interference Cancellation and Iterative Detection for Orthogonal Time Frequency Space Modulation". In: *IEEE transactions on wireless communications* 17.10 (2018), pp. 6501–6515.

[23] Patchava Raviteja, Yi Hong, Emanuele Viterbo, and Ezio Biglieri. "Practical pulse-shaping waveforms for reduced-cyclic-prefix OTFS". In: *IEEE Transactions on Vehicular Technology* 68.1 (2018), pp. 957–961.

[24] Theodore S Rappaport. *Wireless Communications–Principles and Practice*. 2nd. Horizon House Publications, Inc., 2002.

[25] 3GPP. *Study on channel model for frequencies from 0.5 to 100 GHz*. Technical Report TR 38.901, V18.0.0. 3rd Generation Partnership Project (3GPP), 2024.

[26] J. G. Proakis and M. Salehi. *Digital Communications*. 5th. New York, NY, USA: McGraw-Hill, 2008.

[27] 3GPP. *TS 38.104: NR; Base Station (BS) Radio Transmission and Reception*. Version 17.10.0. 3rd Generation Partnership Project, 2023.

[28] 3GPP. *TS 38.211: NR; Physical Channels and Modulation*. Version 17.5.0. 3rd Generation Partnership Project, 2023.

[29] GD Surabhi and A Chockalingam. "Low-complexity linear equalization for OTFS modulation". In: *IEEE communications letters* 24.2 (2019), pp. 330–334.

AUTHORS

Sabbir Ahmed is a doctoral researcher at the Center for Wireless Communications (CWC) at the University of Oulu, Finland, specializing in next generation wireless communication systems. His research focuses on 6G waveform design and optimization, exploring modulation techniques such as Orthogonal Time Frequency Space (OTFS) for high-mobility scenarios. His work encompasses performance analysis of advanced modulation schemes in high-Doppler environments, spectrum efficiency optimization, and the development of intelligent algorithms for adaptive waveform selection in dynamic channel conditions.

Hirley Alves is an associate professor and Head of the Machine-type Wireless Communications Group at the 6G Flagship, part of the Centre for Wireless Communications at the University of Oulu. He leads research on massive connectivity, Ultra-Reliable Low Latency Communications (URLLC), and 5G/6G networks covering areas from machine-type wireless communications and satellite IoT to energy-efficient and goal-oriented communications. He also coordinates massive wireless automation activities within the 6G Flagship and has organized and chaired several international conferences on wireless communications.

Ari Pouttu is a professor and Director of the 6G Flagship program at the University of Oulu, Finland. With over 30 years of experience in information and communication technology, his research spans waveform and system design for military radio communications, radar systems, embedded device networks, and wireless communications from early cellular systems to emerging 6G technologies. He has led numerous projects in cognitive networks, navigation applications, and dependable wireless solutions for various business verticals including security and defence, energy, industry, health, and automotive sectors. Professor Pouttu has authored approximately 100 peer-reviewed publications and holds two patents. From 2006 to 2012, he served as Director of the Centre for Wireless Communications at the University of Oulu. He currently leads a research group focused on experimental networks, including the University's 5G Test Network (5GTN), and actively collaborates on major European initiatives in satellite and terrestrial communications.